High-temperature electronic structure with the Korringa-Kohn-Rostoker Green's function method

C. E. Starrett

High Temperature Electronic Structure with KKR

C. E. Starrett[1, *]

[1]*Los Alamos National Laboratory, P.O. Box 1663, Los Alamos, NM 87545, U.S.A.*
(Dated: April 25, 2018)

Modeling high temperature (10's or 100's of eV), dense plasmas is challenging due to the multitude of non-negligible physical effects including significant partial ionization and multi-site effects. These effects cause the breakdown or intractability of common methods and approximations used at low temperatures, such as pseudopotentials or plane wave basis sets. Here we explore the KKR (Korringa-Kohn-Rostoker) Green's function method at these high temperature conditions. The method is all-electron, does not rely on pseudopotentials, and uses a spherical harmonic basis set, and so avoids the aforementioned limitations. It is found to be accurate for solid density aluminum and iron plasmas when compared to a plane wave method at low temperature, while being able to access high temperatures.

I. INTRODUCTION

Material properties at high temperatures such as equation of state and opacity are used to model a diverse range of physical phenomena such inertial fusion experiments [1], white dwarf stars [2] and main sequence stars [3]. Often density functional theory based average atom models are used to generate the data due to their computational efficiency and reasonable physical fidelity [4–9]. Other higher fidelity methods are available [10, 11], however they have limitations such as extreme computational expense or in which properties can be calculated.

In this work we explore the possibility of using the KKR (Korringa-Kohn-Rostoker) [12–15] Green's function method for equation of state at high temperatures. KKR has been shown to be accurate for total energy calculations at normal conditions [16] but has not yet, to our knowledge, been explored in the literature for high temperature materials (i.e. 10^4 to 10^6 K). This study follows the exploratory work of Wilson *et al* [17] who first demonstrated the possibly of using this method for high temperature materials.

While average atom models have reasonable physical fidelity, one key piece of missing physics is multiple scattering. In average atom models the boundary condition on the electron wavefunctions is that they match the free electron form at the ion sphere. In practice this means that such models assume that scattering electrons are asymptotically free, which is clearly not true in dense materials, where electrons go on to scatter multiple times. This lack of multiple scattering has a significant effect on the calculated electronic structure and hence the predicted material properties.

KKR does include multiple scattering, indeed it is sometimes called multiple scattering theory [14, 18]. The basic idea is that space is partitioned into space-filling, non-overlapping polyhedra. Inside each polyhedron the 'single-site' problem is solved, which amounts to evaluating the Kohn-Sham Density Functional Theory (DFT) equation for the regular and irregular solutions and phase shifts. Then by taking into account the differing frames of reference of each single site solution, the multisite Green's function is constructed [19]. From this Green's function all the usual electronic properties such as EOS and opacity can be calculated [14].

Here we show that an average atom model is a special case of KKR where multiple scattering has been ignored and the polyhedra are approximated as spheres. We then focus on two exploratory example, fcc aluminum and bcc iron at high temperatures. Our use of crystal structures, instead of a disordered fluid structure is justified at this early stage of research in that it is still an improvement over the average atom model, and is useful because it allows us to test a key approximation, that of multiple scattering basis set convergence. Also, such systems, with hot thermal electrons and nuclei at or near their lattice positions, are already of physical interest since they occur in ultra fast heating experiments such as at the X-ray Free Electron Laser facility at LCLS [20].

A further simplification of the present implementation is that we use the Muffin Tin (MT) approximation. In essence this assumes that, for calculating the Green's function, the effective one electron potential is spherically symmetric inside each polyhedron. This is unnecessary in the context of of KKR [21], but does simplify the implementation. Again this is justified at this early stage of research because it allows us to assess the effect of multiple scattering. It is worth noting that even though the MT approximation is used, the electron density is not spherically symmetric in the polyhedra because the multiple scattering boundary condition breaks the symmetry.

The structure of this paper is as follows. In section II we outline the physical model that is being modelled and look at basis set convergence for aluminum and iron plasmas. In section III we show results for equation of state (EOS) and density of states (DOS) for these same aluminum and iron plasmas. We compare to a commonly

---

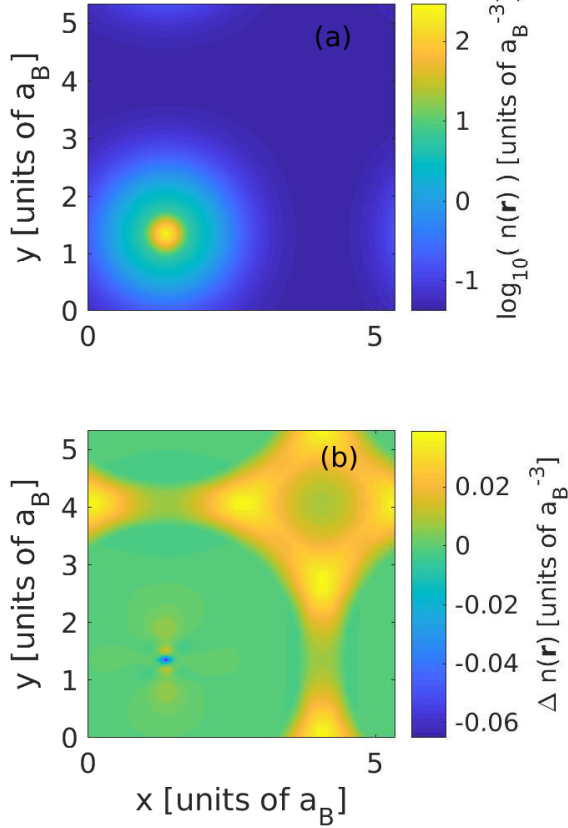*Electronic address: `starrett@lanl.gov`

FIG. 1: (Color online) Top panel: a 2D slice of the 3D electron density $n_e(\boldsymbol{r})$ for bcc iron at solid density and a temperature of 10 eV. Notice the logarithmic colorbar. The electron density is very strongly concentrated at the nuclear position. Bottom panel: the difference Δn_e between $n_e(\boldsymbol{r})$ and the superposition density $n_e^{super}(\boldsymbol{r})$ that must be Fourier transformed to solve the Poisson equation.

used average atom model as well as to state of the art plane-wave DFT calculations. Finally, in section IV we draw our conclusions.

II. PHYSICAL MODEL

We consider dense plasmas in which thermalized electrons move in a background of nuclei that are fixed at their lattice positions. The system is then periodic in the usual way. The electron density $n_e(\boldsymbol{r})$ is found using finite temperature density functional theory [22]. The Free energy functional is

$$F[n_e(\boldsymbol{r})] = F^{KS} + F^{el} + F^{xc} \qquad (1)$$

where F^{KS} is the kinetic-entropic term

$$F^{ks} = U^k - TS \qquad (2)$$

U^k is the electron kinetic energy contribution to the internal energy

$$U^k = \int_{-\infty}^{\infty} d\epsilon f(\epsilon,\mu)\chi(\epsilon)\epsilon - \int_V d^3r V^{eff}(\boldsymbol{r})n_e(\boldsymbol{r}) \qquad (3)$$

and S is the entropy

$$S = -k_B \int_{-\infty}^{\infty} d\epsilon \chi(\epsilon)$$
$$\times [f(\epsilon,\mu)\ln(f(\epsilon,\mu)) + (1 - f(\epsilon,\mu))\ln(1 - f(\epsilon,\mu))] \qquad (4)$$

In these equations μ is the chemical potential found by requiring the system volume V to be charge neutral, ϵ is the energy, $f(\epsilon,\mu)$ is the Fermi-Dirac occupation factor, $\chi(\epsilon)$ is the density of states per volume V and T is the temperature.

F^{el} is the electostatic free energy due to the Coulomb interactions of the nuclei and electron density $n_e(\boldsymbol{r})$ with each other and with themselves. F^{xc} is the exchange and correlation free energy for which we use the temperature independent Perdew-Zunger form [23].

Requiring F to be at a minimum with respect to variations in $n_e(\boldsymbol{r})$ subject to charge neutrality leads to the effective one electron potential

$$V^{eff}(\boldsymbol{r}) = V^{el}(\boldsymbol{r}) + V^{xc}(\boldsymbol{r}) \qquad (5)$$

where $V^{xc}(\boldsymbol{r})$ is the exchange correlation potential and the electrostatic potential is

$$V^{el}(\boldsymbol{r}) = \sum_i \frac{-Z_i}{|\boldsymbol{r} - \boldsymbol{R}_i|} + \int d^3r \frac{n_e(\boldsymbol{r}')}{|\boldsymbol{r} - \boldsymbol{r}'|} \qquad (6)$$

Z_i is the nuclear charge of nucleus i.

This is a self-consistent field problem. The solution procedure is as follows

1. Input nuclear charges and positions, choose electron-exchange and correlation potential, create initial guess at $n_e(\boldsymbol{r})$.

2. Solve Poisson equation for electrostatic potential $V^{el}(\boldsymbol{r})$.

3. Calculate total effective potential $V^{eff}(\boldsymbol{r})$.

4. Solve for an electron density in the presence of $V^{eff}(\boldsymbol{r})$.

5. Mix input and output electron densities to get new input guess and repeat steps 2 to 5 until input and output densities are the same to numerical tolerance.

An example of $n_e(\boldsymbol{r})$ for bcc iron at solid density and a temperature of 10 eV is given in the top panel of figure 1. The figure demonstrates the electron density is very strongly peaked near the nuclei, due to the occupation of bound (or core) states. To solve the Poisson equation a number of options are available [24–27]. We have

opted for the method presented in reference [28] which uses fast-Fourier transforms (FFT) to solve the Poisson equation. This method is suitable for relatively small systems, with perhaps up to a few hundred unique nuclei only. It works by splitting the electron density into a sum of spherically symmetric electron densities placed at each nuclear site $n_e^{super}(\boldsymbol{r}) = \sum_i n_{e,i}^{PA}(r)$ and a correction, $\Delta n_e(\boldsymbol{r}) = n_e(\boldsymbol{r}) - n_e^{super}(\boldsymbol{r})$. The Poisson equation is then solved by using a uniform 3D spatial grid to represent Δn_e, while the potential due to the spherically symmetric quantities is solved for easily using a well known method [28]. An example of the correction density is shown in the bottom panel of figure 1.

To carry out spatial integrals like that in equation (3) we have used the method presented in [29].

To generate a new guess at $n_e(\boldsymbol{r})$ we use the 5th order extended Anderson's method due to Eyert [30, 31]. This is closely related to Broyden's method [32, 33] and typically converges in less than 10 iterations.

All that remains is a method to solve for the electron density. This is where KKR is used.

A. KKR for the electron density

The electron density $n_e(\boldsymbol{r})$ is expressed in terms of the Green's function $G(\boldsymbol{r}', \boldsymbol{r}, \epsilon)$

$$n_e(\boldsymbol{r}) = -\frac{1}{\pi}\Im \int_{-\infty}^{\infty} d\epsilon f(\epsilon, \mu) Tr G(\boldsymbol{r}, \boldsymbol{r}, \epsilon) \qquad (7)$$

where the integral is over energy and non-relativistically the trace amounts to a factor of two that accounts for the spin degeneracy. In KKR, the Green's function is constructed by first partitioning space into non-overlapping polyhedra. For materials with only one type of nucleus we use a Voronoi decomposition, see figure 2. Inside each polyhedron the Schrödinger equation (or Kohn-Sham equation in DFT) is solved using a spherical harmonic $Y_{lm}(\hat{\boldsymbol{r}})$ basis set, resulting in a set of regular $R_l(\epsilon, \boldsymbol{r})$ and irregular $H_l(\epsilon, \boldsymbol{r})$ wavefunctions [34]. These wavefunctions are normalized so that they match free electron behavior at the cell boundaries. This also gives the T-matrix $\underline{t}(\epsilon)$ that is familiar from scattering physics, and is related to the scattering phase shifts. The T-matrix is a matrix in l and m and has size $(l_{max}+1)^2 \times (l_{max}+1)^2$, where l_{max} is the maximum value of l included in the basis set expansion. A super T-matrix is constructed for the N particles in the super cell $\underline{\underline{t}} = \{\underline{t}^{nn'}\delta_{nn'}\}$ where $n = 1, \ldots, N$ labels the nucleus [27].

The positions of the nuclei and the periodic nature of the supercell are then encoded in the so-called structure constants matrix $\underline{G}_0(\epsilon, \boldsymbol{k})$ that accounts for the different origins of the basis sets. $\underline{G}_0$ and $\underline{\underline{t}}$ are combined in the structural Green's function matrix $\underline{\mathscr{G}}(\epsilon)$ [27, 35, 36]. The trace of the Green's function is then written

$$Tr\, G(\boldsymbol{r}, \boldsymbol{r}, \epsilon) = G^{ss}(\boldsymbol{r}, \boldsymbol{r}, \epsilon) + G^{ms}(\boldsymbol{r}, \boldsymbol{r}, \epsilon) \qquad (8)$$
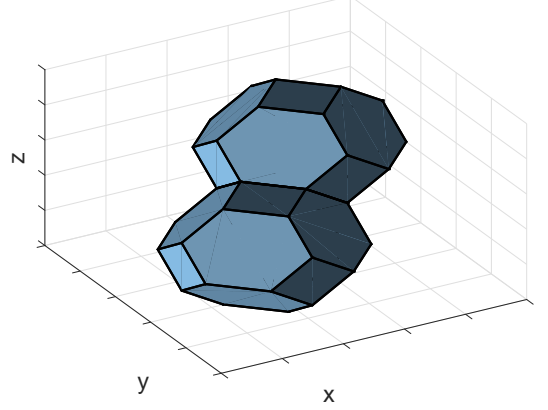

FIG. 2: (Color online) Voronoi decomposition of space around each nuclei here for a bcc crystal. In KKR the Schrödinger equation is solved inside each polyhedron. These solutions together with the positions of the nuclei are then used to construct the Green's function for the entire system, from which the electron density and other material properties are calculated.
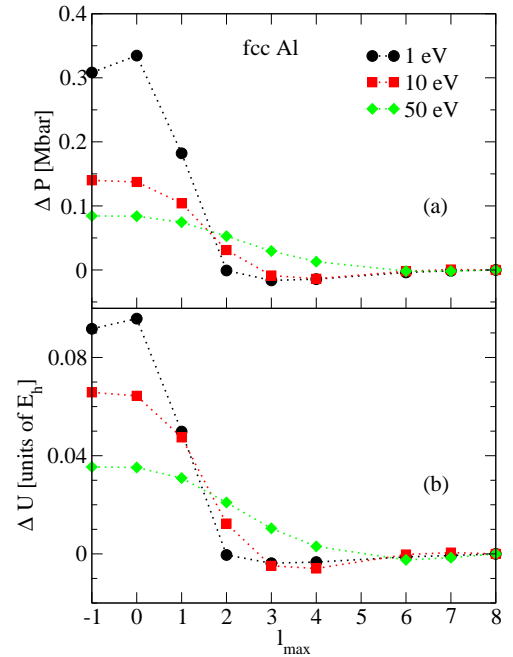

FIG. 3: (Color online) Convergence of changes in pressure ΔP and internal energy ΔU as a function of the truncation of the l summation for G^{ms}, for fcc aluminum.

where the single-site part is

$$G^{ss}(\boldsymbol{r}, \boldsymbol{r}, \epsilon) = -2m\imath\sqrt{2m\epsilon} \sum_{l=0}^{l_{max}} \frac{2(2l+1)}{4\pi} R_l(\epsilon, \boldsymbol{r}) H_l(\epsilon, \boldsymbol{r}'),$$

$$(9)$$

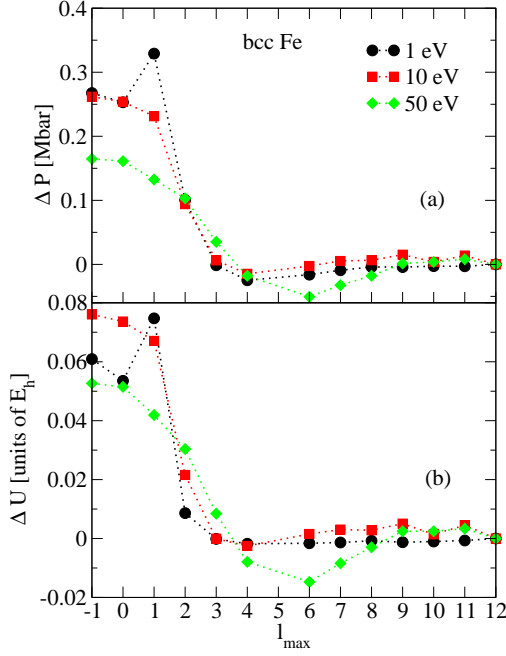with the symbol $\imath$ being the imaginary number, and the

FIG. 4: (Color online) Convergence of changes in pressure ΔP and internal energy ΔU as a function of the truncation of the l summation for G^{ms}, for bcc iron.

multi-site part is

$$G^{ms}(\boldsymbol{r},\boldsymbol{r},\epsilon) = 2m \sum_{l=0}^{l_{max}} \sum_{l'=0}^{l_{max}} \sum_{m=-l}^{l} \sum_{m'=-l'}^{l'} \mathscr{G}_{lml'm'}^{nn}(\epsilon)$$
$$\times R_l(\epsilon,\boldsymbol{r})R_{l'}(\epsilon,\boldsymbol{r})Y_{lm}(\hat{\boldsymbol{r}})Y_{l'm'}^*(\hat{\boldsymbol{r}}) \quad (10)$$

where we have limited ourselves to the local (i.e. $r = r'$) expression and we have assumed that the scattering potential inside each polyhedron is spherically symmetric. This assumption is an approximation that simplifies the numerics but is not formally, or even practically, necessary [21]. To enforce the spherical symmetry we use the common Muffin Tin (MT) approximation. In practice this is done by defining a MT sphere for each polyhedron, which is the largest sphere that completely fits into the polyhedron. Inside the spheres the potential $V^{eff}(\boldsymbol{r})$ is spherically averaged. Outside the spheres, in the so called interstitial region, $V^{eff}(\boldsymbol{r})$ is replaced with its average value $\bar{V}^{MT}$. The total MT potential is then shifted by $\bar{V}^{MT}$ [27]. The Schrödinger equation is then solved for this potential.

This is the only place the MT potential is used, i.e. to generate the Green's function. It is not (directly) used for example, when calculating the equation of state which explicitly depends on the potential $V^{eff}(\boldsymbol{r})$.

It is interesting to note that the single-site and multi-site contributions to the Green's function are fully separable, equation (8). Making the approximation that the multi-site contributions to the Green's function and Poisson equation can be neglected, and approximating the

polyhedra as spheres with volume equal to the average volume per atom, we are left with an average atom model [4, 34, 37]. Such average atom models are widely used for equation of state tables. This derivation brings insight into the approximations and missing physics inherent in average atom models.

The density of states $\chi(\epsilon)$, apprearing in equation (3), is simple related the the Green's function

$$\chi(\epsilon) = -\frac{1}{N\pi}\Im \int_V d^3r \, Tr G(\boldsymbol{r},\boldsymbol{r},\epsilon) \quad (11)$$

where there are N nuclei in the volume V. The pressure is given by the Virial expression

$$P = \frac{1}{V}\left[\frac{\mathscr{T}+F^{el}}{3}\right] + P^{xc} \quad (12)$$

with

$$P_{xc} = \frac{1}{V}\left[-F^{xc} + \int_V d^3r \, n_e(\boldsymbol{r})V^{xc}(\boldsymbol{r})\right] \quad (13)$$

and $\mathscr{T}$ is

$$\mathscr{T} = 2\int_{-\infty}^{\infty} d\epsilon f(\epsilon,\mu)\chi(\epsilon)\epsilon - 2\int_V d^3r V^{eff}(\boldsymbol{r})n_e(\boldsymbol{r}). \quad (14)$$

The internal energy U is

$$U = F^{el} + U^{xc} + U^k \quad (15)$$

where U^{xc} is the exchange and correlation internal energy.

B. Basis Set Truncation

A key question of the method is that of the choice of l_{max}. Since the matrix that has to be inverted has size $N(l_{max}+1)^2$ [38] it is clearly in our interest to keep l_{max} as small as possible. To achieve this we treat l_{max} for G^{ss} and G^{ms} separately. l_{max} for G^{ss} can be numerically converged automatically by the code using a common trick employed in average atom models [39, 40]. l_{max} for G^{ms} determines the size of the matrix to be inverted and can be converged separately through convergence testing. One can expect l_{max} for G^{ms} to converge at much smaller values than that for G^{ss} which for high temperature cases can need $l_{max} > 100$. The reason for this is that electrons in states characterized by large values of l also have higher energies, and therefore behave more like free electrons. Since the t-matrix elements for free electrons are zero, so is G^{ms}.

To test this expectation figures 3 and 4 show convergence of the EOS for fcc aluminum and bcc iron respectively. l_{max} in the figures is that used for G^{ms} only, that for G^{ss} is converged automatically by the code. $l_{max} = -1$ is used to represent the case where $G^{ms} = 0$. For both cases we consider electrons with temperatures
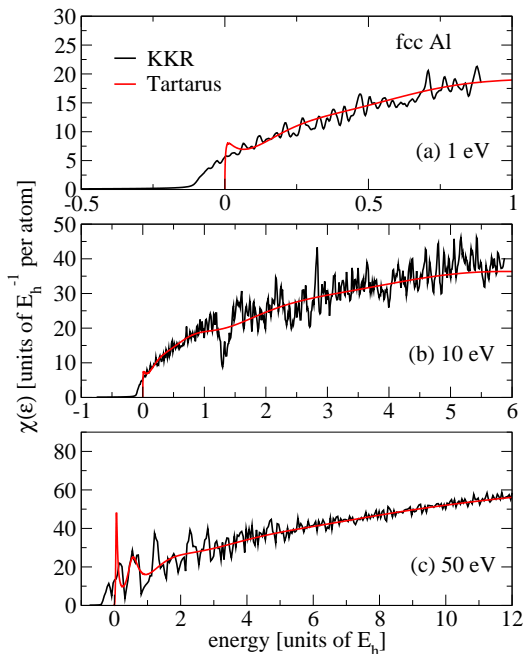
FIG. 5: (Color online) Density of states for fcc aluminum at 2.7 g/cm^3.

FIG. 6: (Color online) Density of states for bcc iron at 7.894 g/cm^3.

of 1, 10 and 50 eV. For all cases the pressure and internal energies are well converged by $l_{max} = 8$. Note that we have plotted absolute changes in pressure and energy, i.e.

$$\Delta P = P(l_{max}) - P(l_{max} = l_{con}) \qquad (16)$$
$$\Delta U = U(l_{max}) - U(l_{max} = l_{con}) \qquad (17)$$

where $l_{con} = 8$ for Al and 12 for Fe. Relative changes would show a relatively small influence of multiple scattering on EOS as temperature is increased (also see figures 7 and 8).

Another interesting feature of these plots is that for iron at 1 eV there is a 'spike' in the EOS changes for $l_{max} = 2$, and rapid convergence thereafter. This is due to capturing the 3d valence band feature in the multiple scattering treatment. This 3d feature is expected to be particularily important at low temperatures, and less so at high temperatures (see later, figure 6).

III. EQUATION OF STATE AND DENSITY OF STATES

In figures 5 and 6 we plot density of states for fcc aluminum and bcc iron respectively. Compared are the DOS from KKR and that from the average atom code Tartarus [40]. Firstly, we note that 'noisy' KKR curves are due to the fact that for real energies the KKR DOS is a series of Dirac delta functions at the eigenvalues of the system. What we actually plot is the real part of the DOS parallel to the real energy axis, with an imaginary part of the energy equal to 0.01 E_h. This effectively broadens the
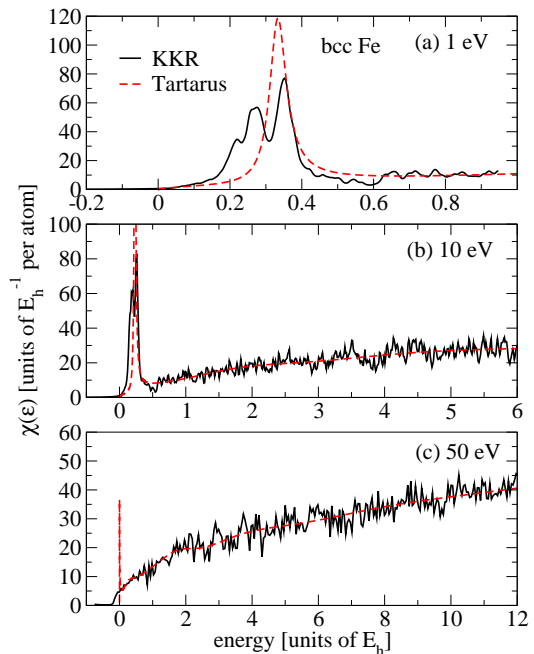
DOS by convolving it with a Lorentzian with a width equal to this imaginary part of the energy [41]. Such noise can also be caused by insufficient k-point sampling. We have converged the shown DOS so that any larger scale features are actual predictions of the model.

Generally speaking, there is a very good level of agreement between the KRR and average atom results. For aluminum at 1 eV the most significant difference is near zero energy where the KKR DOS extends to roughly -0.1 E_h, while the average atom goes to zero at zero energy, as it must. In the average atom model the only states that can appear at negative energies are discrete bound states, whose DOS are Dirac delta functions at the eigenenergy. Clearly KKR does not have this restriction and the DOS looks much more free electron like. Such differences will show up in spectroscopic quantities like opacity. For aluminum at 10 eV one significant difference is a dip in the KKR DOS at 1 to 1.5 E_h in contrast to a very weak dip in the average atom result. At 50 eV for aluminum the KKR DOS displays structure at small energies that is quite different to that displayed by the average atom. Clearly the more realistic treatment of ionic structure and non-spherical symmetry in KKR are the cause of these differences.

For iron, figure 6, the differences are even more pronounced. At 1 eV the large 3d resonance feature in the average atom curve is broadened and reduced in height in KKR. For 10 eV a similar result is seen. By 50 eV the 3d state has recombined and is no longer visible on this scale. The average atom DOS has a large spike at small positive energy associated with a nearly recombined s-
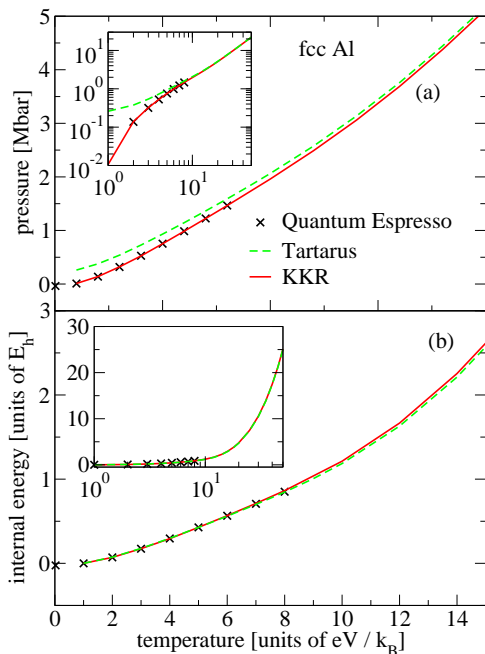
FIG. 7: (Color online) Equation of state of fcc aluminum at solid density.

FIG. 8: (Color online) Equation of state of bcc iron at solid density.

state. This is completely missing from the KKR DOS which is very free electron like.

In summary, there is a good level of general agreement between KKR and average atom but significant differences in details caused by the more realistic treatment of ion structure and non-spherical symmetry in the KKR model.

In figures 7 and 8 EOS from the KKR model is compared to both average atom results and, at low temperatures, to the plane-wave DFT code Quantum Espresso [42, 43] (QE). The QE calculations use pseudopotentials but are thought to be accurate at relatively low temperatures (up to 10 eV here). Moreover, such plane wave type calculations become prohibitively expensive as temperature increases. KKR on the other hand can easily access high temperatures (up to 100 eV here) without significant scaling. Though the calculation of G^{ss} does scale with temperature, the prefactor is small and is not significant for any of the results presented here. Due to the cutoff of l_{max} for G^{ms}, its computational cost does not increase with temperature, hence the quasi-temperature independence of the overall computational cost of the method.

In figure 7 we see very good agreement between the QE and KKR results for both pressure and internal energy, and for higher temperatures, very good agreement between the average atom results and KKR. This is a key result: KKR is accurate at both low and high temperature while remaining computationally feasible. In figure 8, for iron, similar trends are observed. Now however, there are some relatively small differences between the KKR and QE results, presumable due to the muffin-tin
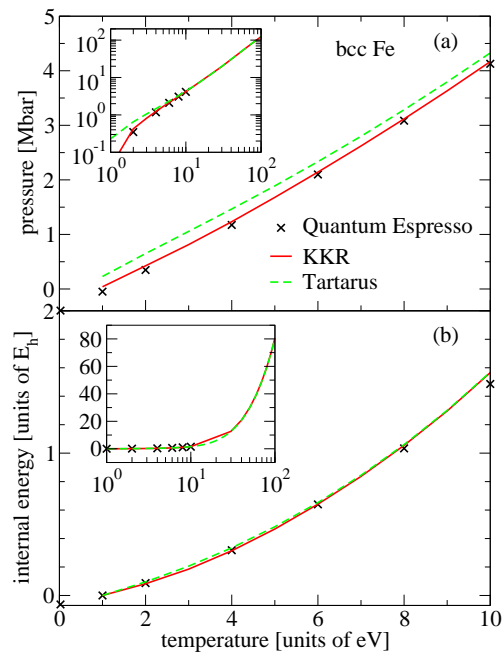
approximation that we have used. Nevertheless, there is a clear and substantial improvement over average atom, particularly for pressure.

IV. CONCLUSION

The KKR method has been explored for use in dense plasmas. It was found that the method is accurate for equation of state when compared to other state of the art methods at low temperature, while being able to access high temperature, partially degenerate, plasma states without prohibitive computational cost. As such, it offers a promising capability to provide high physical fidelity modelling of warm and hot dense plasmas.

It was also shown that the commonly used average atom model is a special case of the KKR method, where multiple scattering has been ignored and the polyhedra around each nucleus approximated by spheres.

Our relatively crude implementation of the method does not exploit many of the numerous methodological and numerical improvements that have been presented over its long history in solid state physics. For example, we have used the obsolete muffin tin approximation due do its relative simplicity to implement. This approximation is unnecessary [21], but is adequate for present purposes. Also, we have used a non-relativistic implementation, but relativity in the form of the Dirac equation is possible [27]. Also, the method can be made to scale linearly with number of particles [44]. In summary, this method offer much promise to improve our under-

standing of warm and hot dense plasmas.

Acknowledgments

The author thanks and T. Sjostrom for doing the Quantum Espresso calculations for this work. This

[1] S. W. Haan, J. D. Lindl, D. A. Callahan, D. S. Clark, J. D. Salmonson, B. A. Hammel, L. J. Atherton, R. C. Cook, M. J. Edwards, S. Glenzer, A. V. Hamza, S. P. Hatchett, M. C. Herrmann, D. E. Hinkel, D. D. Ho, H. Huang, O. S. Jones, J. Kline, G. Kyrala, O. L. Landen, B. J. MacGowan, M. M. Marinak, D. D. Meyerhofer, J. L. Milovich, K. A. Moreno, E. I. Moses, D. H. Munro, A. Nikroo, R. E. Olson, K. Peterson, S. M. Pollaine, J. E. Ralph, H. F. Robey, B. K. Spears, P. T. Springer, L. J. Suter, C. A. Thomas, R. P. Town, R. Vesey, S. V. Weber, H. L. Wilkens, and D. C Wilson. Point design targets, specifications, and requirements for the 2010 ignition campaign on the national ignition facility. *Physics of Plasmas*, 18(5):051001, 2011.

[2] G. Fontaine, P. Brassard, and P. Bergeron. The potential of white dwarf cosmochronology. *Publications of the Astronomical Society of the Pacific*, 113(782):409, 2001.

[3] James E. Bailey, Taisuke Nagayama, Guillaume Pascal Loisel, Gregory Alan Rochau, C. Blancard, J. Colgan, Ph. Cosse, G. Faussurier, C. J. Fontes, F. Gilleron, et al. A higher-than-predicted measurement of iron opacity at solar interior temperatures. *Nature*, 517(7532):56–59, 2015.

[4] B. Wilson, V. Sonnad, P. Sterne, and W. Isaacs. Purgatorio–a new implementation of the inferno algorithm. *J. Quant. Spect. Rad. Trans.*, 99:658, 2006.

[5] R. Piron and T. Blenski. Variational-average-atom-in-quantum-plasmas (VAAQP) code and virial theorem: Equation-of-state and shock-hugoniot calculations for warm dense Al, Fe, Cu, and Pb. *Phys. Rev. E*, 83:026403, Feb 2011.

[6] Gérald Faussurier, Christophe Blancard, Philippe Cossé, and Patrick Renaudin. Equation of state, transport coefficients, and stopping power of dense plasmas from the average-atom model self-consistent approach for astrophysical and laboratory plasmas. *Physics of Plasmas*, 17(5), 2010.

[7] C. E. Starrett and D. Saumon. Electronic and ionic structures of warm and hot dense matter. *Phys. Rev. E*, 87:013104, Jan 2013.

[8] François Perrot and M. W. C. Dharma-wardana. Electrical resistivity of hot dense plasmas. *Phys. Rev. A*, 36:238–246, Jul 1987.

[9] A.A. Ovechkin, P.A. Loboda, and A.L. Falkov. Transport and dielectric properties of dense ionized matter from the average-atom reseos model. *High Energy Density Physics*, 20:38 – 54, 2016.

[10] Burkhard Militzer and Kevin P. Driver. Development of path integral monte carlo simulations with localized nodal surfaces for second-row elements. *Phys. Rev. Lett.*, 115:176403, Oct 2015.

[11] Sebastien Hamel, Lorin X. Benedict, Peter M. Cel-
liers, M. A. Barrios, T. R. Boehly, G. W. Collins, Tilo Döppner, J. H. Eggert, D. R. Farley, D. G. Hicks, J. L. Kline, A. Lazicki, S. LePape, A. J. Mackinnon, J. D. Moody, H. F. Robey, Eric Schwegler, and Philip A. Sterne. Equation of state of $ch_{1.36}$: First-principles molecular dynamics simulations and shock-and-release wave speed measurements. *Phys. Rev. B*, 86:094113, Sep 2012.

[12] J. Korringa. On the calculation of the energy of a bloch wave in a metal. *Physica*, 13(6-7):392–400, 1947.

[13] W. Kohn and N. Rostoker. Solution of the schrödinger equation in periodic lattices with an application to metallic lithium. *Physical Review*, 94(5):1111, 1954.

[14] Hubert Ebert, Diemo Koedderitzsch, and Jan Minar. Calculating condensed matter properties using the KKR-green's function method-recent developments and applications. *Reports on Progress in Physics*, 74(9):096501, 2011.

[15] N. Papanikolaou, R. Zeller, and P.H. Dederichs. Conceptual improvements of the KKR method. *Journal of Physics: Condensed Matter*, 14(11):2799, 2002.

[16] R. Zeller, M. Asato, T. Hoshino, J. Zabloudil, P. Weinberger, and P. H. Dederichs. Total-energy calculations with the full-potential KKR method. *Philosophical Magazine B*, 78(5-6):417–422, 1998.

[17] B. G. Wilson, D. D. Johnson, and Aftab Alam. Multi-center electronic structure calculations for plasma equation of state. *High Energy Density Physics*, 7(2):61–70, 2011.

[18] J.S. Faulkner. Multiple-scattering approach to band theory. *Physical Review B*, 19(12):6186, 1979.

[19] F.S. Ham and B. Segall. Energy bands in periodic latticesgreen's function method. *Physical Review*, 124(6):1786, 1961.

[20] S. M. Vinko, O. Ciricosta, B. I. Cho, K. Engelhorn, H-K. Chung, C. R. D. Brown, T. Burian, J. Chalupský, R. W. Falcone, C. Graves, et al. Creation and diagnosis of a solid-density plasma with an x-ray free-electron laser. *Nature*, 482(7383):59–62, 2012.

[21] Jan Zabloudil. *The full-potential screened KKR method*. PhD Thesis, Technical University, Vienna, 2000.

[22] N. David Mermin. Thermal properties of the inhomogeneous electron gas. *Phys. Rev.*, 137:A1441–A1443, Mar 1965.

[23] John P. Perdew and Alex Zunger. Self-interaction correction to density-functional approximations for many-electron systems. *Physical Review B*, 23(10):5048, 1981.

[24] Aftab Alam, Brian G. Wilson, and Duane D. Johnson. Accurate and fast numerical solution of poisson's equation for arbitrary, space-filling voronoi polyhedra: Near-field corrections revisited. *Physical Review B*, 84(20):205106, 2011.

[25] A. Gonis, Erik C. Sowa, and P. A. Sterne. Exact treatment of poisson's equation in solids with space-filling cells. *Phys. Rev. Lett.*, 66:2207–2210, Apr 1991.

[26] L. Vitos and J. Kollár. Optimized l-convergency in the solution of poisson's equation with space-filling cells. *Phys. Rev. B*, 51:4074–4078, Feb 1995.

[27] Jan Zabloudil, Robert Hammerling, Laszlo Szunyogh, and Peter Weinberger. *Electron Scattering in Solid Matter: a theoretical and computational treatise*, volume 147. Springer Science & Business Media, 2006.

[28] C. E. Starrett. Thomas-fermi simulations of dense plasmas without pseudopotentials. *Phys. Rev. E*, 96:013206, Jul 2017.

[29] Aftab Alam, S. N. Khan, Brian G. Wilson, and D. D. Johnson. Efficient isoparametric integration over arbitrary space-filling voronoi polyhedra for electronic structure calculations. *Phys. Rev. B*, 84:045105, Jul 2011.

[30] V. Eyert. A comparative study on methods for convergence acceleration of iterative vector sequences. *Journal of Computational Physics*, 124(2):271–285, 1996.

[31] Donald G. Anderson. Iterative procedures for nonlinear integral equations. *Journal of the ACM (JACM)*, 12(4):547–560, 1965.

[32] Charles G. Broyden. A class of methods for solving nonlinear simultaneous equations. *Mathematics of computation*, 19(92):577–593, 1965.

[33] D. D. Johnson. Modified broyden's method for accelerating convergence in self-consistent calculations. *Phys. Rev. B*, 38:12807–12813, Dec 1988.

[34] C. E. Starrett. A green's function quantum average atom model. *High Energy Density Phys.*, 16:18, 2015.

[35] Harold L. Davis. Efficient numerical techniques for the calculation of KKR structure constants. In *Computational Methods in Band Theory*, pages 183–199. Springer, 1971.

[36] B Segall. Calculation of the band structure of "complex" crystals. *Physical Review*, 105(1):108, 1957.

[37] David A. Liberman. Self-consistent field model for condensed matter. *Phys. Rev. B*, 20:4981–4989, Dec 1979.

[38] A. Thiess, R. Zeller, M. Bolten, P.H. Dederichs, and S. Blügel. Massively parallel density functional calculations for thousands of atoms: KKRnano. *Physical Review B*, 85(23):235103, 2012.

[39] Thomas Blenski and Kenichi Ishikawa. Pressure ionization in the spherical ion-cell model of dense plasmas and a pressure formula in the relativistic Pauli approximation. *Physical Review E*, 51(5):4869, 1995.

[40] Nathanael Matthew Gill and Charles Edward Starrett. Tartarus: A relativistic greens function quantum average atom code. *High Energy Density Physics*, 24:33–38, 2017.

[41] D. D. Johnson, F. J. Pinski, and G. M. Stocks. Fast method for calculating the self-consistent electronic structure of random alloys. *Phys. Rev. B*, 30:5508–5515, Nov 1984.

[42] Paolo Giannozzi, Stefano Baroni, Nicola Bonini, Matteo Calandra, Roberto Car, Carlo Cavazzoni, Davide Ceresoli, Guido L Chiarotti, Matteo Cococcioni, Ismaila Dabo, Andrea Dal Corso, Stefano de Gironcoli, Stefano Fabris, Guido Fratesi, Ralph Gebauer, Uwe Gerstmann, Christos Gougoussis, Anton Kokalj, Michele Lazzeri, Layla Martin-Samos, Nicola Marzari, Francesco Mauri, Riccardo Mazzarello, Stefano Paolini, Alfredo Pasquarello, Lorenzo Paulatto, Carlo Sbraccia, Sandro Scandolo, Gabriele Sclauzero, Ari P Seitsonen, Alexander Smogunov, Paolo Umari, and Renata M Wentzcovitch. Quantum espresso: a modular and open-source software project for quantum simulations of materials. *Journal of Physics: Condensed Matter*, 21(39):395502 (19pp), 2009.

[43] P Giannozzi, O Andreussi, T Brumme, O Bunau, M Buongiorno Nardelli, M Calandra, R Car, C Cavazzoni, D Ceresoli, M Cococcioni, N Colonna, I Carnimeo, A Dal Corso, S de Gironcoli, P Delugas, R A DiStasio Jr, A Ferretti, A Floris, G Fratesi, G Fugallo, R Gebauer, U Gerstmann, F Giustino, T Gorni, J Jia, M Kawamura, H-Y Ko, A Kokalj, E Kkbenli, M Lazzeri, M Marsili, N Marzari, F Mauri, N L Nguyen, H-V Nguyen, A Otero de-la Roza, L Paulatto, S Ponc, D Rocca, R Sabatini, B Santra, M Schlipf, A P Seitsonen, A Smogunov, I Timrov, T Thonhauser, P Umari, N Vast, X Wu, and S Baroni. Advanced capabilities for materials modelling with quantum espresso. *Journal of Physics: Condensed Matter*, 29(46):465901, 2017.

[44] Rudolf Zeller. Linear scaling for metallic systems by the Korringa-Kohn-Rostoker multiple-scattering method. In *Linear-Scaling Techniques in Computational Chemistry and Physics*, pages 475–505. Springer, 2011.